AD-A130 980 MICROSTRUCTURE AND PROPERTIES OF P/M TOOL STEELS(U) 1/1
DREXEL UNIV PHILADELPHIA PA DEPT OF MATERIALS
ENGINEERING S KUMAR ET AL. JUN 83 N00014-81-K-0039
UNCLASSIFIED F/G 7/4 NL

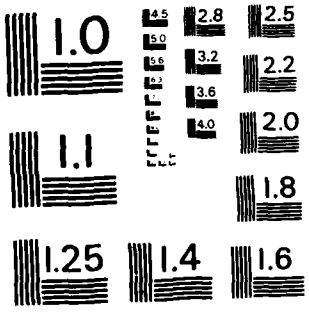

TECHNICAL REPORT
Contract N00014-81-K0039

MICROSTRUCTURE AND PROPERTIES OF P/M TOOL STEELS

S. Kumar, A. Fareed, M.J. Koczak and A. Lawley
Department of Materials Engineering
Drexel University
Philadelphia, PA 19104

June 1983

Office of Naval Research
Materials Division
800 N. Quincy Street
Arlington, VA 22217

Unclassified

SECURITY CLASSIFICATION OF THIS PAGE (When Data Entered)

REPORT DOCUMENTATION PAGE	READ INSTRUCTIONS BEFORE COMPLETING FORM
1. REPORT NUMBER	2. GOVT ACCESSION NO. A130 980	3. RECIPIENT'S CATALOG NUMBER
4. TITLE (and Subtitle) Microstructure and Properties of P/M Tool Steels	5. TYPE OF REPORT & PERIOD COVERED Technical Report
	6. PERFORMING ORG. REPORT NUMBER
7. AUTHOR(s) S. Kumar, A. Fareed, M.J. Koczak and A. Lawley	8. CONTRACT OR GRANT NUMBER(s) N00014-81-K0039
9. PERFORMING ORGANIZATION NAME AND ADDRESS Drexel University Department of Materials Engineering Philadelphia, PA 19104	10. PROGRAM ELEMENT, PROJECT, TASK AREA & WORK UNIT NUMBERS
11. CONTROLLING OFFICE NAME AND ADDRESS Department of the Navy Materials Division, Office of Naval Research Arlington, VA 22217	12. REPORT DATE June 1983
	13. NUMBER OF PAGES 26
14. MONITORING AGENCY NAME & ADDRESS(if different from Controlling Office)	15. SECURITY CLASS. (of this report) Unclassified
	15a. DECLASSIFICATION/DOWNGRADING SCHEDULE

16. DISTRIBUTION STATEMENT (of this Report)

DISTRIBUTION STATEMENT A
Approved for public release;
Distribution Unlimited

17. DISTRIBUTION STATEMENT (of the abstract entered in Block 20, if different from Report)

18. SUPPLEMENTARY NOTES

19. KEY WORDS (Continue on reverse side if necessary and identify by block number)

Tool Steel Powder Atomization; Powder Characterization; Powder Consolidation; Heat treatment; Microstructures; Mechanical Properties.

20. ABSTRACT (Continue on reverse side if necessary and identify by block number)

A detailed microstructural examination has been made of T15 and Rex 25 high speed tool steels processed from rapidly solidified gas atomized powders, and associated strength and toughness evaluated. Powders were screened into selected size fractions, hot isostatically pressed to full density and heat-treated. Two HIPing temperatures, two austenitizing temperatures and three tempering temperatures were included in the study.

DD FORM 1 JAN 73 1473 EDITION OF 1 NOV 65 IS OBSOLETE

Unclassified

SECURITY CLASSIFICATION OF THIS PAGE (When Data Entered)

Atomized and consolidated materials were characterized utilizing x-ray diffraction, optical and scanning electron microscopy. Both cellular and dendritic structures are present in the atomized powders depending on particle size, with MC carbides present primarily at cell boundaries. After HIPing, MC, M_6C and $M_{23}C_6$ carbides are present in the form of individual particles in a ferritic matrix. Independent of prior particle size fraction, the carbide size distribution after HIPing is skewed to larger carbide sizes with increasing HIPing temperature, but with no significant change in volume fraction of carbides. $M_{23}C_6$ goes into solution during austenitizing if the temperature is high enough, and it does not reprecipitate on tempering. Austenite grain size and the volume fraction and size distribution of MC and M_6C carbides are controlled primarily by the prior HIPing and austenitizing temperatures; the trends observed after HIPing are maintained after heat-treatment. Strength and toughness are enhanced by hot forging after HIPing but prior to heat-treatment; the effect is more pronounced in the finer particle size fractions. Property levels are either equal or superior to those of the corresponding commercial P/M tool steel. The dependence of property levels on powder characteristics and processing parameters is understood in terms of the associated microstructures.

PROGRESS IN POWDER METALLURGY, VOLUME 39 - IN PRESS

MICROSTRUCTURE AND PROPERTIES OF P/M TOOL STEELS

S. Kumar, A. Fareed, M.J. Koczak and A. Lawley
Department of Materials Engineering
Drexel University
Philadelphia, Pa. 19104

Abstract

A detailed microstructural examination has been made of T15 and Rex 25 high speed tool steels processed from rapidly solidified gas atomized powders, and associated strength and toughness evaluated. Powders were screened into selected size fractions, hot isostatically pressed to full density and heat-treated. Two HIPing temperatures, two austenitizing temperatures and three tempering temperatures were included in the study. Atomized and consolidated materials were characterized utilizing x-ray diffraction, optical and scanning electron microscopy. Both cellular and dendritic structures are present in the atomized powders depending on particle size, with MC carbides present primarily at cell boundaries. After HIPing, MC, M_6C and $M_{23}C_6$ carbides are present in the form of individual particles in a ferritic matrix. Independent of prior particle size fraction, the carbide size distribution after HIPing is skewed to larger carbide sizes with increasing HIPing temperature, but with no significant change in volume fraction of carbides. $M_{23}C_6$ goes into solution during austenitizing if the temperature is high enough, and it does not reprecipitate on tempering. Austenite grain size and the volume fraction and size distribution of MC and M_6C carbides are controlled primarily by the prior HIPing and austenitizing temperatures; the trends observed after HIPing are maintained after heat-treatment. Strength and toughness are enhanced by hot forging after HIPing but prior to heat-treatment; the effect is more pronounced in the finer particle size fractions. Property levels are either equal or superior to those of the corresponding commercial P/M tool steel. The dependence of property levels on powder characteristics and processing parameters is understood in terms of the associated microstructures.

Introduction

Powder metallurgy (P/M) high speed tool steels have been a commercial reality for over a decade. Compared to their ingot metallurgy (I/M) counterparts, the P/M tool steels exhibit superior alloying homogeneity coupled with fine grain size and a uniformity and fineness of carbide dispersions that cannot be achieved by conventional casting and working processes. The microstructural characteristics of the P/M material are reflected in improved grindability, bend strength, tool life and consistent machinability. In addition, a smaller out-of-roundness occurs during heat-treatment compared to the I/M product; this is a consequence of the relatively isotropic microstructure of the P/M tool steels.

Commercial P/M tool steels are consolidated from gas atomized powder covering a broad particle size range, typically up to 1200 μm. Thus a wide range of cooling rates is inherent in the powders prior to consolidation, with the finer powder particle size falling in the rapid solidification regime. Since the structure of high speed steel is extremely sensitive to cooling rate (1-3), it is clear that a spectrum of microstructures is present in commercial high speed tool steel powders prior to consolidation. Further, the extent to which the structures in the atomized powder are retained during hot isostatic pressing will depend on the prior particle cooling rate and consolidation temperature.

The results and observations presented here provide an understanding of (i) the effect of cooling rate, including the rapid solidification regime, on powder particle microstructures, (ii) microstructural changes accompanying hot isostatic pressing of the powder and (iii) processing-microstructure-property/performance relations as a function of prior particle size. Two high speed steel compositions were included, T15 and Rex 25; the latter is a cobalt free version of T15 with similar heat-treatment response, mechanical properties and tool performance. The atomized powders were screened into narrow size ranges in order to obtain the required spectrum of cooling rates.

Experimental Procedures

Microstructural Analysis

Heats of T15 and Rex 25 tool steels were nitrogen gas atomized and the powder was collected in liquid nitrogen at the base of the atomizing unit. Chemical analysis of the two batches of powder are summarized in Table I. The levels of the alloying elements were similar to those in commercial (CPM) T15 and Rex 25 tool steels. Powders evaluated in the present study were < 2000 μm in size.

T15 and Rex 25 powders of selected size fractions were characterized in the as-atomized condition in terms of their microstructure, microhardness and constituent phases, utilizing scanning electron microscopy, transmission electron microscopy of two stage replicas, and x-ray diffraction.

Bars of each alloy from four size ranges (≤ 840 μm, 250-840 μm, 44-100 μm and ≤ 44 μm) were HIPed at 1195°C or 1130°C. The higher temperature is that used by Crucible Inc. for its commercial CPM high speed tool steels. The lower temperature was used as a possible means for controlling grain size and carbide size during densification. Heat treatment studies of pieces cut from the HIPed

Table I: Compositions of P/M High Speed Tool Steels (weight %)

Alloy	Alloy Form	C	Cr	Co	W	V	Mo
T15	Powder/This Program	1.52	4.67	5.22	12.19	4.85	----
Rex 25	Powder/This Program	1.79	3.01	----	13.29	4.63	6.52
T15	Powder/Commercial	1.48	4.00	4.59	12.12	4.65	0.58
Rex 25	Powder/Commercial	1.81	4.04	0.48	12.46	4.95	6.48

bars included two austenitizing temperatures (1176°C and 1225°C) and three tempering temperatures (538°C, 552°C and 565°C). For convenience, the HIPing, austenitizing and tempering temperatures are coded in Table II.

Table II: Coding System for Powder Consolidation and Heat Treatment

Code	Interpretation
H1	Hot Isostatically Pressed at 1130°C (2065°F)
H2	Hot Isostatically Pressed at 1195°C (2185°F)
A1	Austenitized at 1176°C (2150°F) for 4 mins. and oil-quenched
A2	Austenitized at 1226°C (2240°F) for 4 mins. and oil-quenched
T1	Tempered for (2 + 2 + 2) hrs. at 538°C (1000°F)
T2	Tempered for (2 + 2 + 2) hrs. at 552°C (1025°F)
T3	Tempered for (2 + 2 + 2) hrs. at 565°C (1050°F)

Compacts corresponding to the coarsest and finest size fractions and the two HIPing temperatures were polished, etched and examined by SEM. This was also done following heat treatment of the samples. For purposes of identification, carbides were chemically extracted from the consolidated and the consolidated and heat-treated material (4). Carbide volume fractions, sizes and size distributions were determined by means of a combination of selective etching (4) and quantitative metallography.

Mechanical Properties

T15 and Rex 25 powders of five size fractions (≤ 1200 μm, 250-350 μm, 105-180 μm, 63-105 μm, ≤ 44 μm) were HIPed at 1130°C (H1) into cylindrical compacts (2 per size fraction) approximately 3" diameter and 9.5" in height. One

HIPed compact from each size fraction was hot forged at 1125°C. The compacts were initially converted from a round cylinder to a square shape using a ¼" reduction per pass. After the compacts were square, the amount of reduction per pass was decreased to 1/8". The final cross-sectional dimension of the forged material was approximately 1.375" x 1.375".

C-notch Charpy impact (5) and four-point bend tests (6) were carried out on the coarsest and finest size fractions (250-350 μm and ≤ 44 μm) from each alloy after HIPing (H1) and heat treating (A2 + T2), as well as after HIPing (H1), hot forging and heat treating (A2 + T2).

Results and Observations

Microstructure

Atomized Powder: Polished and etched powder cross-sections from three size fractions (550-700 μm, 110-130 μm, ≤ 37 μm for T15 and 840-2000 μm, 62-74 μm, ≤ 37 μm for Rex 25) were examined by high resolution SEM. Representative micrographs are shown in Figures 1, 2, 3 and 4 for T15 and 5, 6, 7 and 8 for Rex 25. For T15, in the 550-700 μm size fraction, there is a cellular structure in which the cells are outlined by a discontinuous network of carbides, Figure 1; needles of martensite are visible in the matrix. Figure 2 shows the microstructure of the 110-130 μm size fraction. A cellular structure is again evident but the cell size is much smaller and the carbide network more continuous than in the coarser size fraction, cf. Figures 1 and 2. In several locations, particularly at the junction of three cells, the carbide structure has a morphology ("script-carbides") characteristic of eutectic solidification, Figures 1 and 2.

The microstructure of the < 37 μm screen size powder is illustrated in Figures 3 and 4. In some particles a predominantly dendritic mode of solidification is evident (Figure 3) while in others, the cellular structure characteristic of the coarser size fraction is seen, Figure 4. In the latter, the cell size is similar to that in the 110-130 μm size fraction. Similar structural characteristics are evident in Rex 25, Figures 5, 6, 7 and 8.

For both T15 and Rex 25, Debye-Scherrer diffraction patterns of extracted carbides from each size fraction were consistent with the presence of cubic and hexagonal MC carbides. X-ray diffraction of atomized T15 powders from each size fraction shows the matrix to be a mixture of retained austenite and martensite.

Consolidated Material: Micrographs (SEM) of polished and etched samples corresponding to the coarsest (840-250 μm) and finest (≤ 44 μm) size fractions are shown in Figures 9 through 12 for T15 and Figures 13 through 16 for Rex 25. For both alloys, the carbides are coarser following HIPing at the higher temperature (H2). For a given HIPing temperature (H1 or H2), the carbide size is essentially independent of prior particle size fraction. In T15, the matrix consists of α ferrite and three carbides are present, namely cubic MC, cubic M_6C and cubic $M_{23}C_6$. In Rex 25, the situation is similar except that $M_{23}C_6$ was not identified.

EDAX spectra showing typical compositions of MC and M_6C carbides are illustrated in Figure 17(a) and 17(b) for T15 and 18(a) and 18(b) for Rex 25. MC carbides are vanadium rich, and contain only a limited amount of tungsten; in

contrast, M_6C carbides are rich in tungsten, iron and molybdenum. It has been found that the degree to which these elements are present in the carbides is a function of the HIPing temperature.

Carbide volume fractions are summarized in Table III as a function of particle size fraction and HIPing temperature.

Table III: Carbide Volume (%) as a Function of Powder Size Fraction and HIPing Temperature

Alloy	Size Fraction	Carbide Type	H1	H2
T15	250-840 μm	MC	16.2 ± 1.8*	17.9 ± 2.2
T15	≤ 44 μm	MC	14.4 ± 1.2	14.1 ± 1.3
T15	250-840 μm	M_6C	16.7 ± 3.7	16.6 ± 2.2
T15	≤ 44 μm	M_6C	17.5 ± 1.5	15.2 ± 3.3
Rex 25	250-840 μm	MC	12.8 ± 0.6	14.9 ± 0.6
Rex 25	≤ 44 μm	MC	12.9 ± 3.0	9.8 ± 2.9
Rex 25	250-840 μm	M_6C	32.9 ± 5.3	34.7 ± 2.7
Rex 25	≤ 44 μm	M_6C	30.1 ± 4.4	25.8 ± 1.3

*Standard Deviation

For both carbides, the volume fraction is not a sensitive function of powder size fraction or HIPing temperature. Representative carbide size distributions in Rex 25 are given in Figures 19 through 22. For both MC and M_6C carbides, the size distribution is skewed to higher carbide size with an increase in HIPing temperature, cf. Figures 19 and 20, 21 and 22. The extent of the skew is greater for M_6C carbides than for MC carbides. A similar trend exists for MC and M_6C carbides in T15. No selective etching technique exists for the unambiguous and quantitative identification of $M_{23}C_6$.

Heat-Treated Material: Austenitized and quenched samples of T15 were polished and etched to delineate the prior austenite grain boundaries. Representative optical micrographs are shown for the coarsest (840-250 μm) and finest (≤ 44 μm) size fractions for the conditions H1 + A1, H1 + A2, H2 + A1 and H2 + A2 in Figures 23, 24, 25, 26, 27 and 28. An increase in the austenitizing temperature causes an increase in the prior austenite grain size, cf. Figures 23 and 24, 25 and 26, 27 and 28. Similarly, the HIPing temperature influences the austenite grain size; a lower HIPing temperature results in a smaller grain size, cf. Figures 23 and 25, 24 and 26. A comparison of Figures 23 with 27 and 24 with 28 shows that the prior particle size fraction has no significant influence on the austenite grain size.

Analysis of diffraction traces from extracted carbides (T15) confirms the presence of MC and M_6C at each stage of heat-treatment. Some $M_{23}C_6$ remains

after austenitizing at A1, but all this carbide is dissolved at A2. $M_{23}C_6$ does not reprecipitate during tempering. No new carbide-types have been identified after heat-treatment.

Volume fractions of MC and M_6C carbides after HIPing and HIPing, austenitizing and quenching are compared for T15 in Figures 29 and 30. For both MC and M_6C, the amount of carbides going into solution increases with increasing austenitizing temperature. Prior particle size fraction has little influence on the extent of carbide dissolution. HIPing temperature influences the amount of carbides in the quenched material; MC carbides (Figure 29) in the 250-840μm size fraction exhibit a higher volume fraction after H1 + A2 than after H2 + A2. Such a difference is not observed for the M_6C carbides, Figure 30. In the case of M_6C carbides the corresponding volume fractions are similar. Figures 31 and 32 compare the M_6C carbide size distribution for the 250-840 μm screen fraction after H1 + A2 and after H2 + A2. For similar volume fractions of M_6C carbides, a finer size distribution is observed for samples after H1 + A2 than after H2 + A2.

Polished and etched T15 samples in the HIPed and heat-treated conditions were examined by high resolution SEM. Representative micrographs are shown in Figures 33, 34 and 35 for the coarsest size fraction (250-840 μm) and Figures 36, 37 and 38 for the finest (≤ 44 μm) size fraction. For both size fractions, a martensitic matrix is observed after austenitizing and quenching (Figures 33 and 36). Subsequent tempering produces a tempered martensitic structure (Figures 34, 35, 37 lnd 38). No visible microstructural difference exists as a function of prior particle size fraction.

Figures 39 and 40 are x-ray diffraction patterns that illustrate the tempering response of the T15 material corresponding to the coarsest size fraction (250-840 μm). The broad peaks in the austenitized and quenched condition (Figures 39a and 40a) correspond to a mixture of retained austenite and martensite. Complete resolution of the martensite, retained austenite and MC carbide peaks could not be achieved. Subsequent tempering results in the formation of a ferrite matrix and therefore a decrease in peak width (Figures 39b, c and 40b, c). Further, a visible shift in the position of the ferrite peak is observed on tempering as well as with increasing tempering temperature, cf. Figure 39a with 39b, 39b with 39c, 40a with 40b and 40b with 40c.

Volume fraction data for M_6C and MC carbides in T15 tool steel, as a function of prior particle size fraction, HIPing temperature and heat treatment (A, T) are given in Tables IV and V, respectively.

Table IV: Volume (%) of M_6C as a Function of Heat Treatment for T15 Tool Steel

Size Fraction	A1	A1 + T1	A1 + T2	A1 + T3	A2	A2 + T1	A2 + T2	A2 + T3
250-840 μm (H1)	--	---	---	---	5.2	5.3	8.4	7.4
250-840 μm (H2)	6.7	7.2	8.7	9.6	5.4	6.1	7.5	8.4
≤ 44 μm (H1)	--	---	---	---	4.9	7.6	7.2	9.7
≤ 44 μm (H2)	6.9	8.6	8.3	10.4	--	4.5	7.2	7.4

Table V: Volume (%) of MC as a Function of Heat-Treatment for T15 Tool Steel

Size Fraction	A1	A1 + T1	A1 + T2	A1 + T3	A2	A2 + T1	A2 + T2	A2 + T3
250-840 μm (H1)	--	---	---	---	12.8	11.8	12.7	11.5
250-840 μm (H2)	9.7	10.5	12.7	11.3	8.7	11.9	11.3	11.4
≤ 44 μm (H1)	--	---	---	---	11.9	12.2	13.9	10.9
≤ 44 μm (H2)	10.9	9.3	9.8	11.9	--	11.8	12.4	9.9

From Table IV, it is seen that the volume fraction of M_6C carbides increases with increasing tempering temperature. This effect is not as pronounced for the MC carbides (Table V). Prior particle size fraction and HIPing temperature do not influence the volume fraction of MC or M_6C carbides following heat treatment. The size distribution of the carbides is, however, influenced by the HIPing temperature, cf. Figures 41 and 42 and 43 and 44. The size distribution is skewed to the coarser carbide sizes (for similar heat-treatment) for the higher HIPing temperature.

Mechanical Properties

Strength: Bend fracture stress and total deflection at fracture are summarized in Table VI for T15 and Rex 25 processed according to the sequence H1 + A2 + T2. Test data for commercial CPM T15 (corresponding to a ≤ 1200 μm powder blend) are included in Table VI.

Table VI: Bend Fracture Stress and Total Deflection as a Function of Powder Size and Processing

Alloy	Size Fraction	HIPed + Heat-Treated		HIPed + Hot-Worked** + Heat-Treated	
		Bend Fracture Strength (ksi)	Total Deflection (inches)x10^{-4}	Bend Fracture Strength (ksi)	Total Deflection (inches)x10^{-4}
T15*	Commercial (≤ 1200 μm)	---	---	446 ± 45	352 ± 40
T15	250 - 350 μm	420 ± 25	369 ± 25	510 ± 30	458 ± 50
T15	≤ 44 μm	418 ± 40	372 ± 40	567 ± 5	486 ± 10
Rex 25	250 - 350 μm	417 ± 80	318 ± 50	457 ± 50	369 ± 24
Rex 25	≤ 44 μm	457 ± 40	378 ± 20	537 ± 30	417 ± 33

*Commercial CPM T15 is HIPed at H2 and subsequently worked by hot rolling and heat treated v'a A2 + T2.
**For d sampl were evaluated in the longitudinal direction.

For T15 and Rex 25 forging increases both the bend fracture stress and total deflection, compared to the HIPed condition, Table VI. In both alloys, the fine size fraction (≤ 44 μm) exhibits a higher fracture stress and total deflection compared to the coarse size fraction (250-350 μm). Values of bend fracture stress for the commercial material are lower than those quoted in the literature (7). Under similar testing conditions the fracture stress of the coarse and fine size fractions are equal to or greater than that of the commercial CPM material, Table VI.

Toughness: Impact values for T15 and Rex 25 are listed in Table VII. For purposes of comparison, impact toughness values from literature for commercial CPM T15 and Rex 25 have been included.

Table VII: C-Notch Impact as a Function of Powder Size Fraction and Processing†

Alloy	Size Fraction	Consolidated and Heat Treated (ft-lb)	Consolidated, Worked and Heat Treated (ft-lb)
T15 (Commercial)	≤ 1200 μm	---	14.0*
T15	250 - 350 μm	8.7 ± 0.6	15.2 ± 0.4
T15	≤ 44 μm	9.8 ± 0.3	15.8 ± 0.5
Rex 25 (Commercial)	≤ 1200 μm	---	9.5*
Rex 25	250 - 350 μm	8.8 ± 2.2	9.6 ± 0.6
Rex 25	≤ 44 μm	9.5 ± 0.8	12.9 ± 0.4

†Average of 3 samples.
*From literature, reference 7.

For a particular size fraction, in both T15 and Rex 25, the HIPed, forged and heat treated material exhibits superior toughness compared to the HIPed and heat-treated material. For T15 and Rex 25 similar toughness values were obtained in the coarse and fine size fractions in the HIPed and heat-treated condition. The HIPed, forged and heat-treated T15 material does not exhibit appreciable differences in toughness as a function of prior particle size fraction; the fine size fraction in Rex 25 does, however, exhibit a higher toughness than the coarse size fraction. Impact values from the literature(7) for commercial CPM T15 and Rex 25 are similar to or lower than the values obtained in the present study for the coarse and fine size fractions.

Discussion

Microstructure

Atomized Powder: In gas atomization, a stream of liquid metal is broken-up by means of a high pressure gas stream. The resulting liquid droplets spheroidize in free fall before solidification due to surface tension. Particle collisions can occur before and/or after solidification (3) and this is responsible for satellite formation. Cubic MC and hexagonal γ-MC carbides have been identified in all the powder size fractions examined. γ-MC is not present in the HIPed material. This implies that γ-MC is not an equilibrium phase but is present in the atomized powder as a result of the high cooling rate. During the HIPing cycle, γ-MC goes into solution and/or reverts to the cubic form. From Figures 1 and 2, it appears that austenite nucleates first on solidification. The solute-rich liquid solidified later at the γ cell boundaries and there is evidence for eutectic decomposition, e.g. Figures 1, 2 and 5.

With increasing rates of particle cooling (i.e. smaller particle size), higher degrees of undercooling result in a higher nucleation rate of austenite, and hence a smaller cell size, Figures 2 and 6. The transition from a cellular to a dendritic mode of solidification with decreasing particle size (cf. Figure 2 with Figure 3 and Figure 6 with Figure 7) can be explained in terms of the cooling rate T, the thermal gradient G, and the solid/liquid interface velocity, R. Similar observations have been reported by Smugeresky (8). Levi and Mehrabian (9) have pointed out that as the droplet size decreases, the time for the start and completion of solidification decreases, the interface velocity at equivalent fractions solidified increases, and the G to R ratio decreases. Consequently as the droplet size and the G to R ratio decreases, a change from a cellular to a dendritic structure can be expected. The presence of a cellular structure in some of the particles in the < 37 μm screen fraction is possibly due to the fact that some of these fine particles spend a longer time in the turbulent gas zone during atomization; in consequence, they experience a decrease in the extent of undercooling.

Needles of martensite are visible in the coarsest size fraction but are not evident in the finer powder particles. This can be explained in terms of the high degree of supersaturation of the austenite associated with higher cooling rates in the < 37 μm particles (3).

Consolidated Material: After HIPing, MC, M_6C and $M_{23}C_6$ carbides are present in T15. This is to be expected since the slow cooling rates inherent in the HIP cycle leave the consolidated material essentially in the annealed condition. These carbides are known to be present after annealing (4). Only MC and M_6C were identified after HIPing in Rex 25. The absence of $M_{23}C_6$ is attributed to the relatively low amount of chromium (3 wt%) in the steel resulting in too small a fraction of $M_{23}C_6$ to be detected. A comparison of Figures 9, 10, 11 and 12 for T15 and Figures 13, 14, 15 and 16 for Rex 25 shows that for a particular HIPing temperature, the carbides are approximately the same size. However, the carbides are coarser following HIPing at the higher temperature due to enhanced diffusion of the alloying elements.

From Table III, for T15 and Rex 25, the carbide volume fractions are similar for the two HIPing temperatures evaluated. This implies that equilibrium levels of solubility have been achieved at both HIPing temperatures. For similar volume fractions, the skewing of the carbide size distribution to a coarser size at H2 implies a smaller number fraction of carbides at the higher HIPing temperature, cf. Figures 19 with 20 and 21 with 22. The extent of the skew is

greater for M_6C than for MC and is attributed to the higher stability of the latter.

Heat-Treated Material: The increase in austenite grain size with increasing austenitizing temperature (cf. Figures 23 and 24, 25 and 26 and 27 and 28) is due to the larger amount of carbides going into solution at the higher temperature. These carbides at the grain boundaries serve as grain growth inhibitors. Thus, progressive dissolution of these carbides allows for grain growth.

For similar austenitizing temperatures, the HIPing temperature influences the austenite grain size; samples HIPed at H1 and austenitized at A1 exhibit a finer austenite grain size compared to those HIPed at H2 and austenitized at A1, cf. Figures 23 and 25. A similar argument holds for samples austenitized at A2, cf. Figures 24 and 26. This is understood in terms of the microstructural changes taking place in the as-atomized powder during heating to the HIPing temperature, holding at the HIPing temperature, slow cooling to ambient, and subsequently austenitizing. Specifically, the final result in terms of austenite grain size reflects the interplay of MC and M_6C carbide precipitation, dissolution and growth on volume fraction, and the distribution of carbide sizes by number and volume.

In T15, the presence of traces of $M_{23}C_6$ after austenitizing at A1 confirms that this temperature is not high enough to dissolve all of this type of carbide which was present after HIPing. The solution of $M_{23}C_6$ supplies carbon to the austenite matrix and makes it amenable to quench hardening. Therefore, maximum strengthening of the matrix requires a higher austenitizing temperature than A1, e.g. A2 at which all the $M_{23}C_6$ is dissolved. On this basis, a combination of HIPing at H1 and austenitizing at A2 was selected for subsequent mechanical property evaluation in the present study.

From Figure 29 it can be seen that MC carbides go into solution on austenitizing and the volume of MC carbides going into solution increases with increasing austenitizing temperature. Further, for similar powder size fractions, HIPing temperature influences the volume fraction of MC carbides that go into solution on austenitizing. Samples HIPed at H1 and austenitized at A2 exhibit a higher volume fraction of MC carbides than those HIPed at H2 and austenitized at A2, Figure 29. A possible interpretation of this behavior is that for similar volume fraction of MC carbides, the material HIPed at H2, exhibits a size distribution skewed to the coarser side. This in turn implies a larger inter-carbide distance in the sample HIPed at H2. In this sample the presence of coarse and fine carbides, together with a larger intercarbide distance, causes accelerated dissolution of the fine carbides. In the sample HIPed at H1, the size distribution is more narrow and therefore a correspondingly lower, more uniform rate of dissolution. This feature is not observed for the M_6C carbides which are not as stable as the MC carbides, Figure 30. In comparison to MC, a larger fraction of M_6C dissolves on austenitizing. Here too, the amount of M_6C carbides that go into solution, increases with increasing austenitizing temperature. The volume fraction of M_6C carbides present after austenitizing and quenching is not a sensitive function of the HIPing temperature.

The presence of a more narrow M_6C carbide size distribution and smaller average carbide size after H1 + A2 than after H2 + A2 for the 250-840 μm screen fraction (cf. Figures 31 and 32) is a direct consequence of the finer size distribution obtained after HIPing at H1 as compared to H2.

Analysis of diffraction traces from extracted carbides confirmed the presence of MC and M_6C carbides on tempering. No new carbide-types were

identified on tempering.

The tempering response was monitored by x-ray diffraction, Figures 39 and 40. In the austenitized and quenched condition, martensite and retained austenite were present. However, the twin peaks from BCT martensite, (110) and (011), could not be resolved. The retained austenite peak, (111), also lies very close to the MC carbide peak and could not be resolved, Figures 39a and 40a. However, a comparison of Figures 39a with 39b and 40a with 40b shows a decrease in the retained austenite + MC carbide peak on tempering. Since MC carbides precipitate on tempering the peak observed in the quenched condition must include retained austenite. The decrease in peak width on tempering confirms the transformation of martensite to alloyed ferrite and carbides. The visible shift in the position of the ferrite peak to higher angles with increasing tempering temperature is explained in terms of the decrease in the alloy content of the ferrite and concurrent formation of MC and M_6C carbides, cf. Figures 39b with 39c and 40b with 40c. Increasing the austenitizing temperature from A1 to A2 results in a higher volume fraction of carbides going into solution. This enriches the austenite martix in alloying elements and carbon. The net effect is a lowering of the M_S temperature and therefore a decrease in the amount of martensite in the samples quenched from A2 as compared to A1; a reverse trend holds for the amount of retained austenite. These effects are reflected in Figures 39a and 40a; for similar half-peak widths, the peak height is lower for martensite after austenitizing at A2 (Figure 40a) than after austenitizing at A1 (Figure 39a).

Volume fraction data for M_6C and MC carbides as a function of tempering temperatures are given in Tables IV and V, respectively. On tempering, the excess carbon precipitates from the supersaturated matrix in the form of MC or M_6C carbides. The volume fraction of M_6C increases with increasing tempering temperature due to the matrix relieving its supersaturation with respect to carbon and carbide forming elements.

Taking account of the limits of uncertainty (± standard deviation), in most cases a small increase in the volume fraction of MC carbides is observed as a function of tempering temperature. MC carbides are vanadium-rich and the amount of MC carbides that goes into solution during austenitizing is small compared to M_6C. This implies that matrix supersaturation with respect to vanadium is small and therefore the driving force for MC precipitation during tempering is low. Figure 29 shows that the amount of MC carbide is a function of HIPing temperature; the volume fraction of MC carbides after H1 + A2 is greater than after H2 + A2. Thus after processing at H1 + A2, the matrix is less supersaturated with respect to vanadium than after processing at H2 + A2. Thus the driving force for MC carbide precipitation is higher in the latter situation (H2 + A2). This argument is substantiated by the volume fraction data in Table V. There is, however only a very gradual increase in volume fraction of MC carbides with increasing tempering temperature. The effect of HIPing temperature on the size distribution of MC and M_6C carbides after tempering is reflected in Figures 41, 42, 43 and 44. Although the size distribution of MC carbides in the heat-treated samples is relatively independent of the HIPing temperature, the size distribution of M_6C is not. No matter what heat treatment was used, samples HIPed at H1 have about 60-65% by volume of M_6C carbides in the 0.6-1.2 μm range. Samples HIPed at H2 and subsequently heat-treated have 45-50% of the total M_6C volume fraction lying in the size range 1.2-1.8 μm. This behavior emphasizes the importance of the HIPing temperature as a processing parameter and its effect on the microstructure of the heat treated material.

Mechanical Properties

Strength: For both alloy compositions, samples tested in the HIPed and heat-treated conditions exhibit bend strengths which are independent of prior particle size fraction. This is to be expected as no appreciable difference was observed in the microstructures of the coarse and fine size fraction after consolidation.

Of technological importance is the improvement in bend strength of T15 and Rex 25 by secondary hot working (forging), independent of powder size fraction. Further, for each steel, the increase in bend strength is significantly higher for the finer size fraction, Table VI. It has been shown in this study that the carbides present, carbide volume fraction and carbide size distribution are similar for the fine or coarse powder size fractions after HIPing (H1). Further, after austenitizing (A2), the grain size is similar for the fine and coarse powder size fractions. Preliminary fractographic studies reveal a trans particle morphology for both size fractions. Hence, it is tentatively proposed that the enhancement in bend strength achieved via hot forging is related to the presence of microporosity in the HIPed material. In particular, for the narrow size fractions examined in this study, it is possible that the severity of microporosity will be greater for the finer size fraction because of poor powder flow and particle bridging during canning. Consequently, subsequent hot deformation should have a preferred effect on the healing of microporosity in material from the finer particle size fraction.

Toughness: For T15, toughness is independent of prior particle size fraction in the HIPed + heat-treated and HIPed + heat-treated + hot forged material. There is, however, a marked increase (~65%) in toughness for both size fractions as a result of hot forging, Table VII. In Rex 25, toughness does not change significantly with powder particle size after HIPing + heat-treatment. Corresponding increases in toughness after hot forging are ~ 10% and ~ 35% in the coarse and fine size fractions, respectively.

The increase in toughness with increase in bend strength is consistent with the known response of relatively brittle materials. Here, strength is a sensitive function of microstructural integrity and any microporosity, inclusions, or poor particle-particle bonding will reflect in lower strength and toughness. Failure is related to resistance to crack initiation rather than subsequent propagation. The total carbide volume fractions after HIPing in T15 ($V_f \sim 0.33$) is lower than that in Rex 25 ($V_f \sim 0.5$). Assuming that the extent of carbide dissolution at the forging temperature is the same in both T15 and Rex 25, the former should experience more deformation and material flow, by virtue of the smaller fraction of MC and M_6C carbides present. This would explain the larger increase in toughness observed in the T15 tool steel.

Conclusions

1. In both T15 and Rex 25, the microstructure of the atomized powder is dependent on particle size and hence on particle cooling rates. The structure varies from cellular in the coarse powder size fraction to a combination of cellular and dendritic in the fine size fractions. Cubic and hexagonal MC carbides are present in the atomized powder; the hexagonal form is metastable.

2. HIPing temperature is critical in controlling the microstructure of the heat-treated steels in terms of austenite grain size and carbide size

distribution. A lower HIPing temperature (H1) results in a finer austenite grain size and a finer carbide size distribution. The volume fraction of carbides is, however, insensitive to the HIPing temperature (H1 or H2).

3. Prior particle size fraction does not influence the microstructure or the mechanical properties of the HIPed and heat-treated material.

4. Introduction of an intermediate hot forging step leads to an increase in strength and toughness in both steels, independent of prior particle size fraction. The magnitude of the increase is, however larger for the finer size fraction.

5. Strength and toughness levels of both the coarse and fine size fraction processed via the sequence H1 + hot forge + A2 + T2 are either equal or superior to those of the commercial CPM material.

Acknowledgments

This research is supported by the Office of Naval Research. The authors wish to thank Dr. B.A. MacDonald and Dr. D.E. Polk for their cooperation, interest, and involvement in the program.

References

1. I.R. Sare and R.W.K. Honeycombe, Metal Science, Vol. 13, p. 269, 1979.

2. J.J. Rayment and B. Cantor, Met. Trans. Vol. 12A, p. 1557, 1981.

3. H.F. Fischmeister, A.D. Ozerskii and L. Olsson, Powder Metallurgy, Vol. 25, #1, p. 1, 1982.

4. D.J. Blickwede, M. Cohen and G.A. Roberts, Trans. ASM, Vol. 42, p. 1161, 1950.

5. G. Steven, Metal Progress, Vol. 75, p. 76, 1959.

6. A.H. Grobe and G.A. Roberts, Trans. ASM, Vol. 40, p. 435, 1948.

7. W.T. Haswell, W. Stasko and F.R. Dax in Processing and Properties of High Speed Tool Steels, Editors: M.G.H. Wells and L.W. Lherbier, The Metallurgical Society of AIME, Warrendale, PA, p. 147, 1980.

8. J.E. Smugeresky, Met. Trans., Vol. 13A, p. 1535, 1982.

9. C.J. Levi and R. Mehrabian, Met. Trans., Vol. 11B, p. 21, 1980.

Figure 1. As-atomized T15 powder, 550-700 µm; Kalling's etch. SEM.

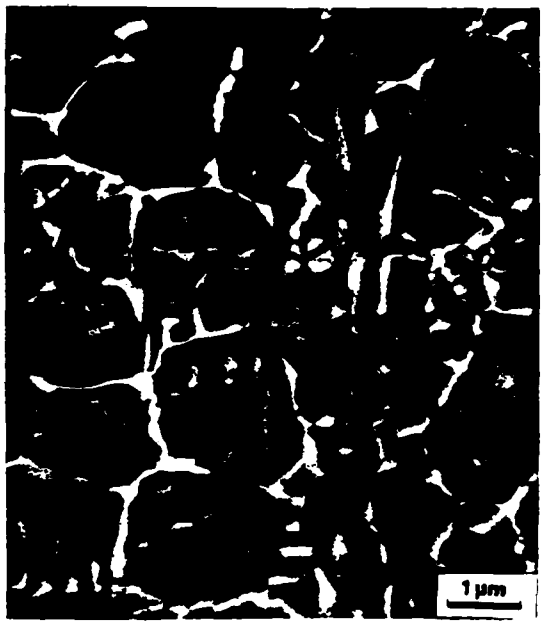

Figure 2. As-atomized T15 powder, 110-130 µm; Kalling's etch. SEM.

Figure 3. As-atomized T15 powder, ≤ 37 µm; Kalling's etch. SEM.

Figure 4. As-atomized T15 powder, ≤ 37 µm; Kalling's etch. SEM.

Figure 5. As-atomized Rex 25 powder, 840-2000 µm; Kalling's etch. SEM.

Figure 6. As-atomized Rex 25 powder, 62-74 µm; Kalling's etch. SEM.

Figure 7. As-atomized Rex 25 powder, ≤ 37 µm; Kalling's etch + HCl-picral. SEM.

Figure 8. As-atomized Rex 25 powder, ≤ 37 µm; Kalling's etch + HCl-picral. SEM.

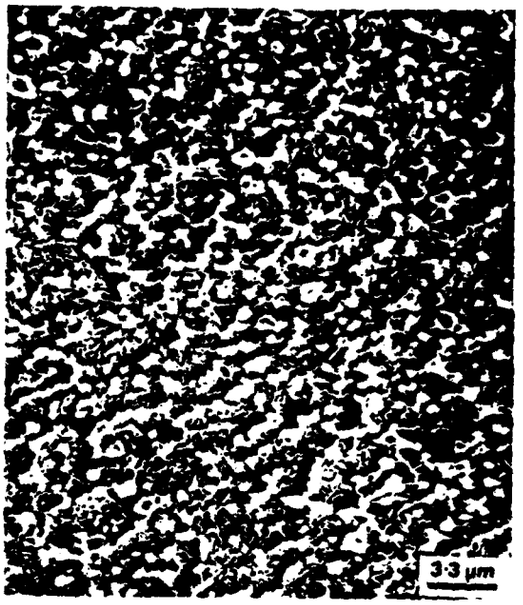

Figure 9. HIPed (H1)/250-840 µm screen (T15); Kalling's etch. SEM.

Figure 10. HIPed (H1)/≤ 44 µm screen (T15); Kalling's etch. SEM.

Figure 11. HIPed (H2)/250-840 µm screen (T15); Kalling's etch. SEM.

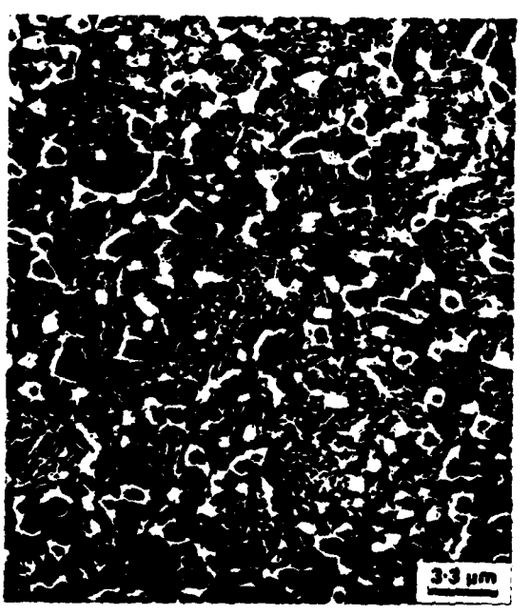

Figure 12. HIPed (H2)/≤ 44 µm screen (T15); Kalling's etch. SEM.

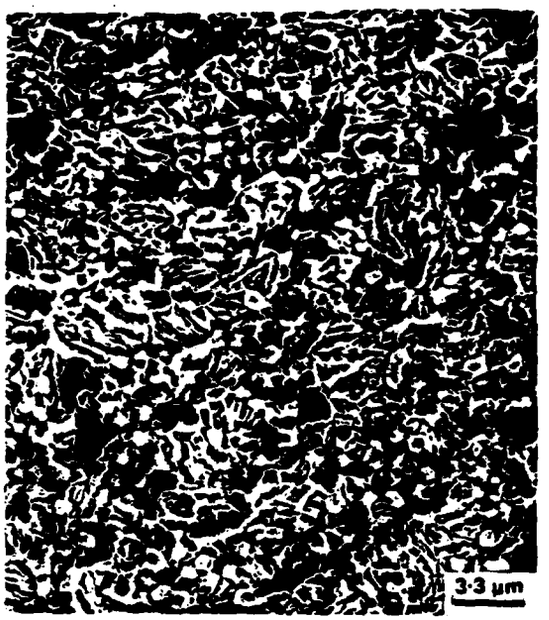

Figure 13. HIPed (H1)/250-840 µm screen (Rex 25); Kalling's etch. SEM.

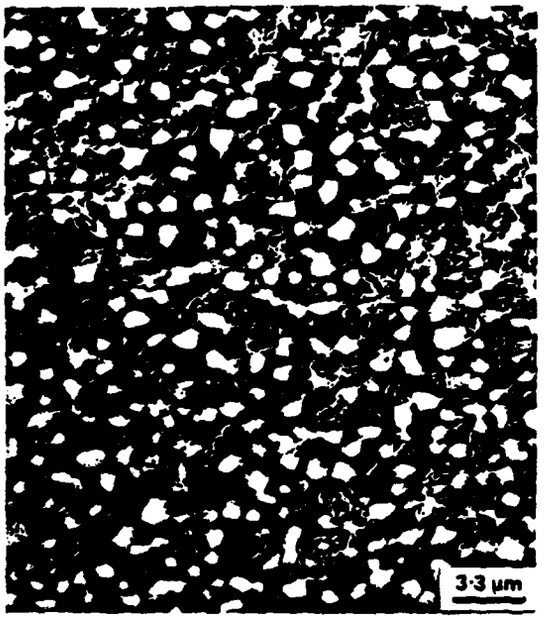

Figure 14. HIPed (H1)/≤ 44 µm screen (Rex 25); Kalling's etch. SEM.

Figure 15. HIPed (H2)/250-840 µm screen (Rex 25); Kalling's etch. SEM.

Figure 16. HIPed (H2)/≤ 44 µm screen (Rex 25); Kalling's etch. SEM.

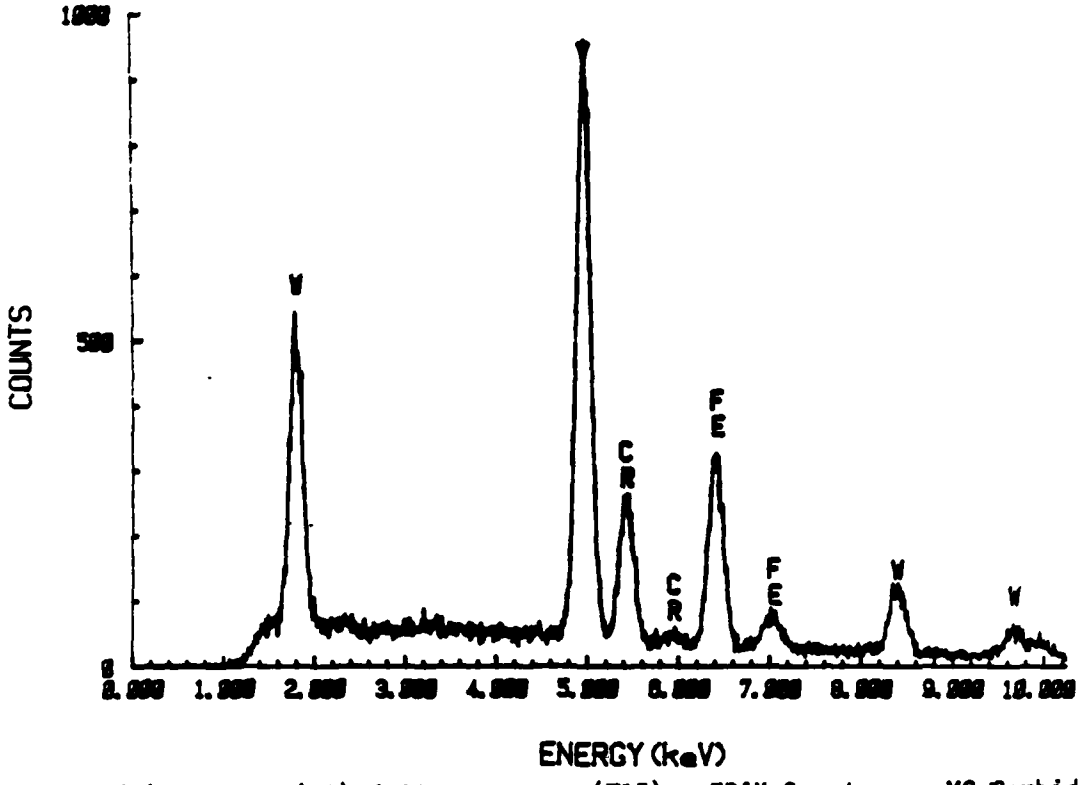

Figure 17(a). HIPed (H2)/≤ 44 μm screen (T15). EDAX Spectrum - MC Carbides.

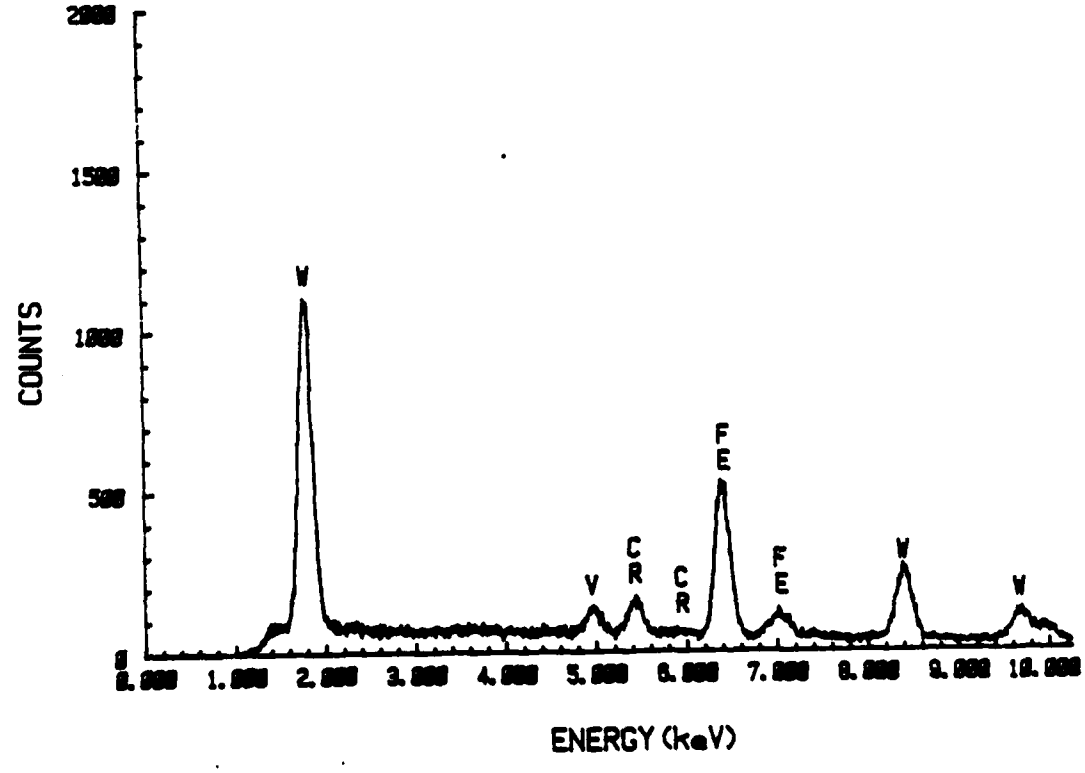

Figure 17(b). HIPed (H2)/≤ 44 μm screen (T15). EDAX Spectrum - M_6C Carbides.

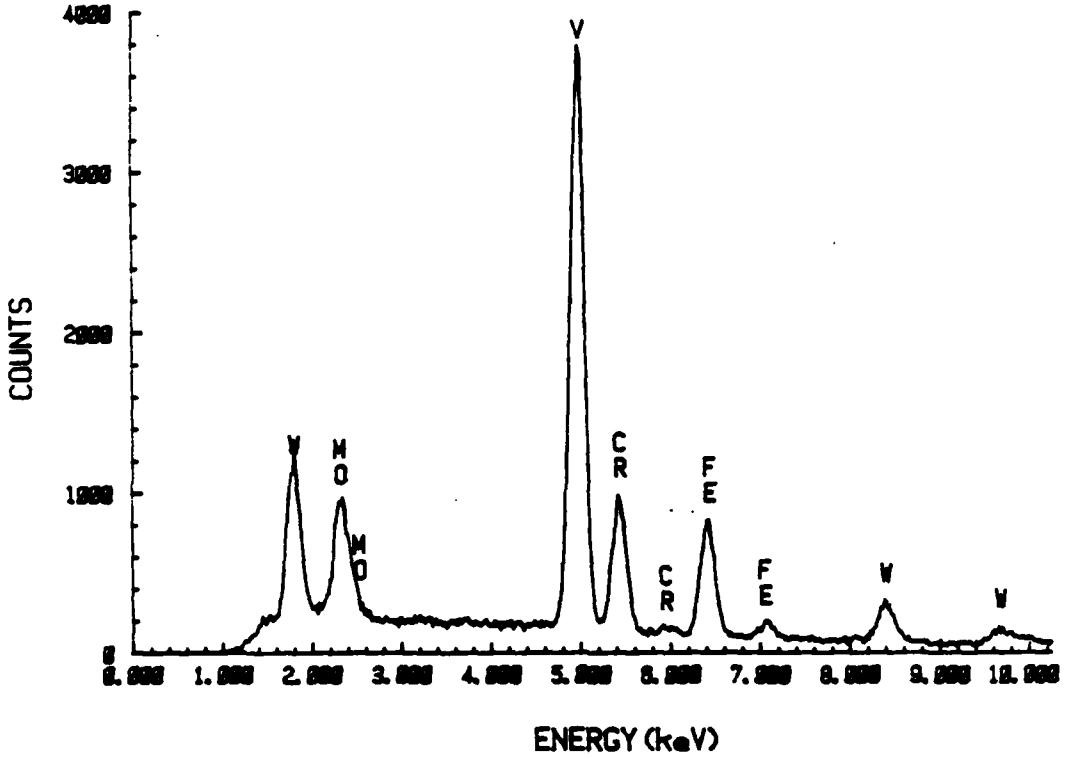

Figure 18(a). HIPed (H2)/≤ 44 μm screen (Rex 25). EDAX Spectrum - MC Carbides.

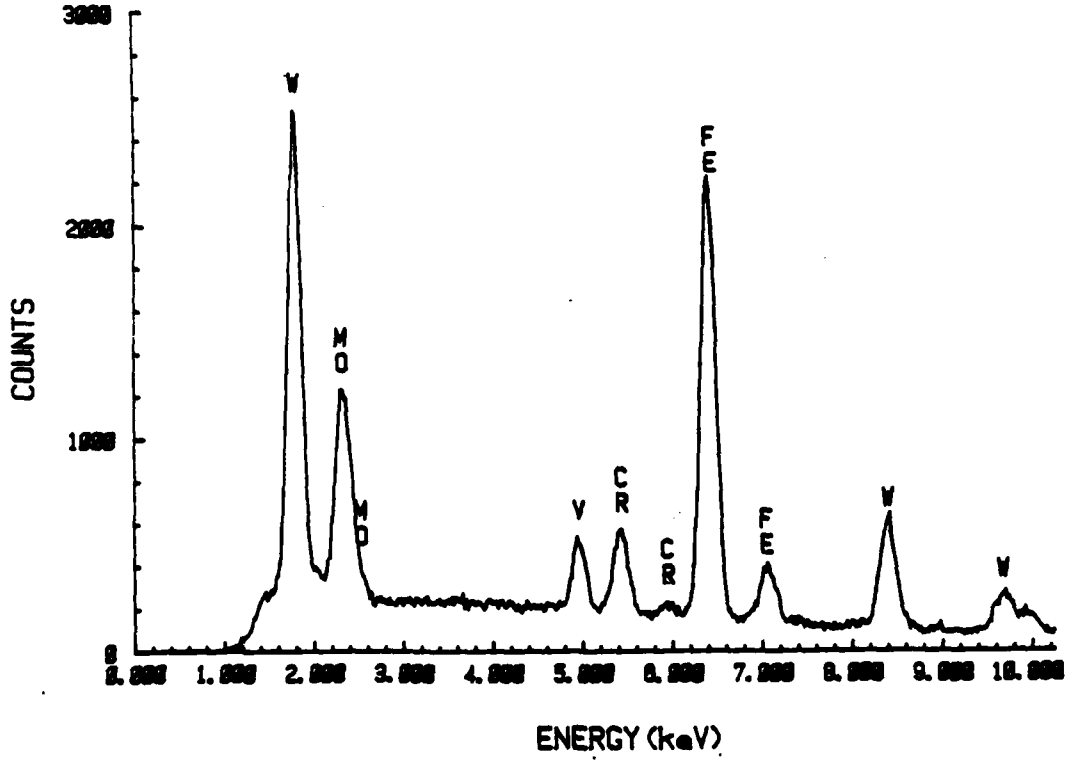

Figure 18(b). HIPed (H2)/≤ 44 μm screen (Rex 25). EDAX Spectrum - M_6C Carbides.

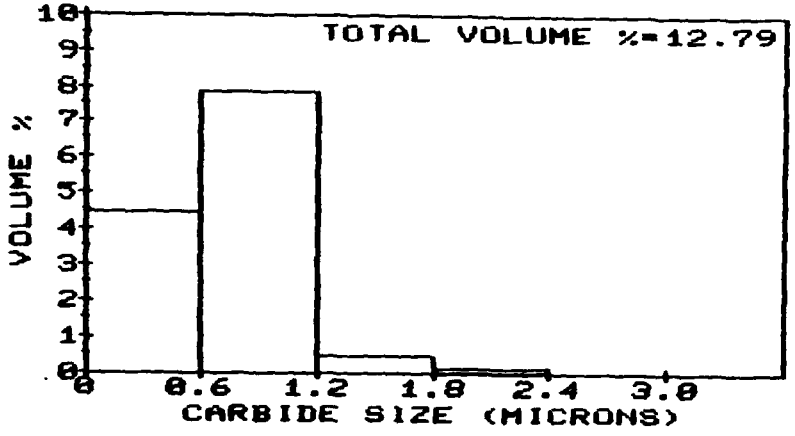

Figure 19. Size distribution - MC; H1/250-840 µm screen (Rex 25).

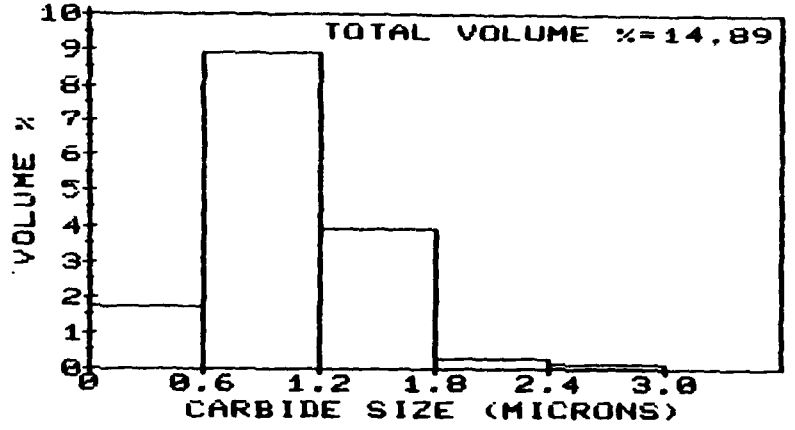

Figure 20. Size distribution - MC; H2/250-840 µm screen (Rex 25).

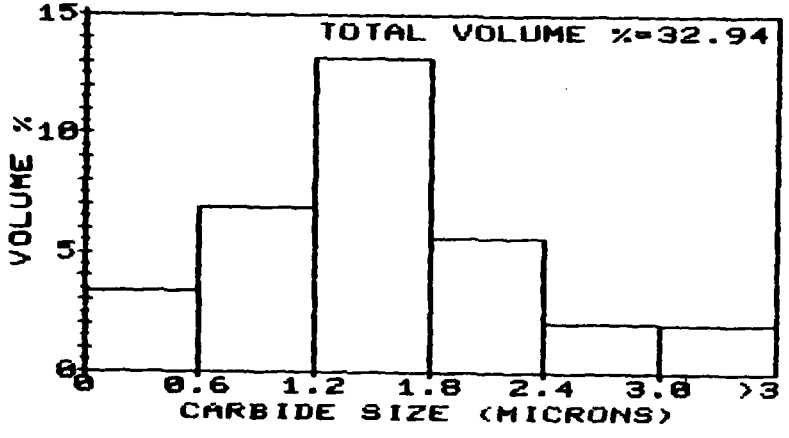

Figure 21. Size distribution - M_6C; H1/250-840 µm screen (Rex 25).

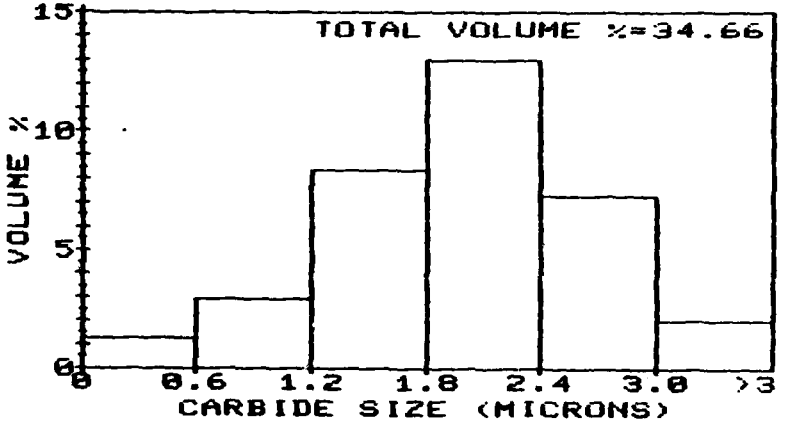

Figure 22. Size distribution - M_6C; H2/250-840 µm screen (Rex 25).

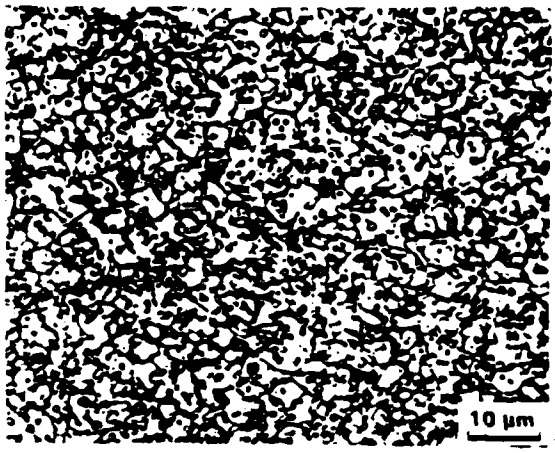

Figure 23. Heat-treated material; H1 + A1/ 250-840 µm screen (T15), 10% Nital.

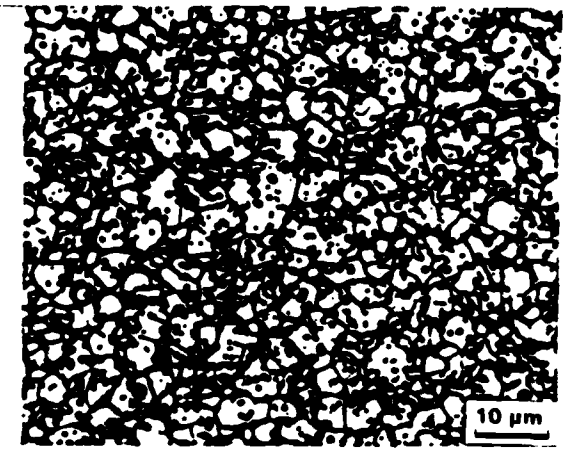

Figure 24. Heat-treated material; H1 + A2/250-840 µm screen (T15), 10% Nital.

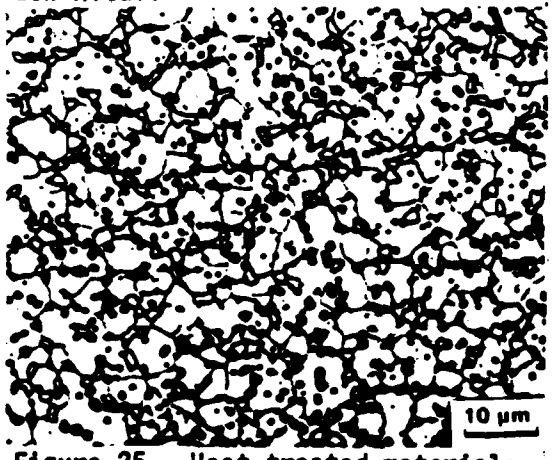

Figure 25. Heat-treated material; H2 + A1/250-840 µm screen (T15), 10% Nital.

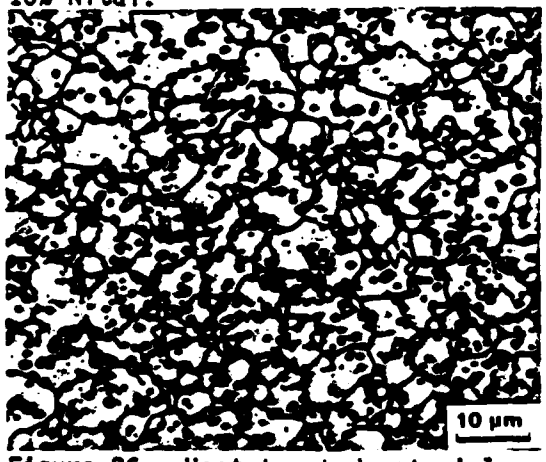

Figure 26. Heat-treated material; H2 + A2/250-840 µm screen (T15), 10% Nital.

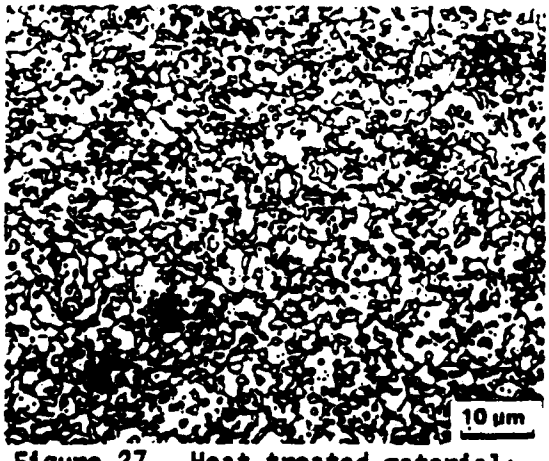

Figure 27. Heat-treated material; H1 + A1/≤ 44 µm screen (T15), 10% Nital.

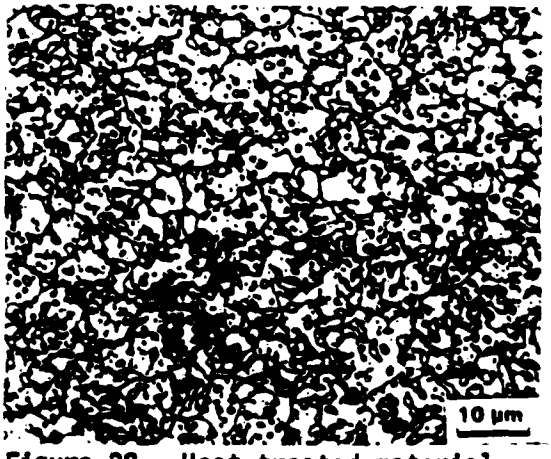

Figure 28. Heat-treated material; H1 + A2/≤ 44µm screen (T15), 10% Nital.

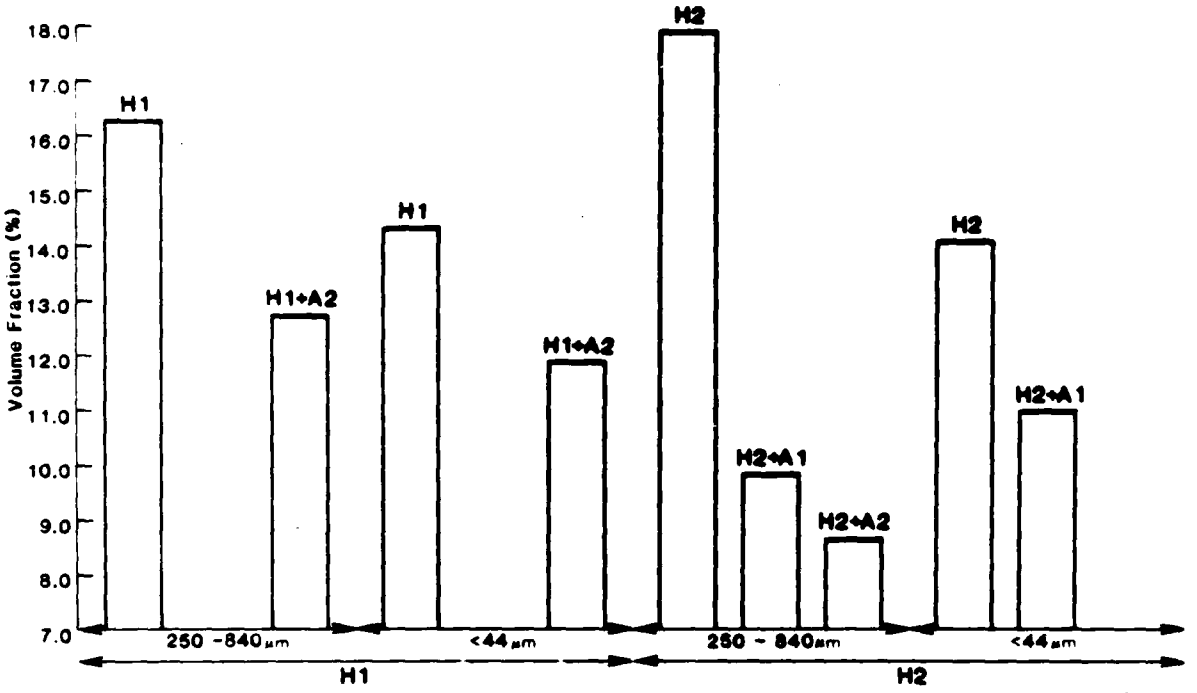

Figure 29. MC Carbide volume fraction (T15) as a function of powder screen fraction, HIPing temperature and austenitizing temperature.

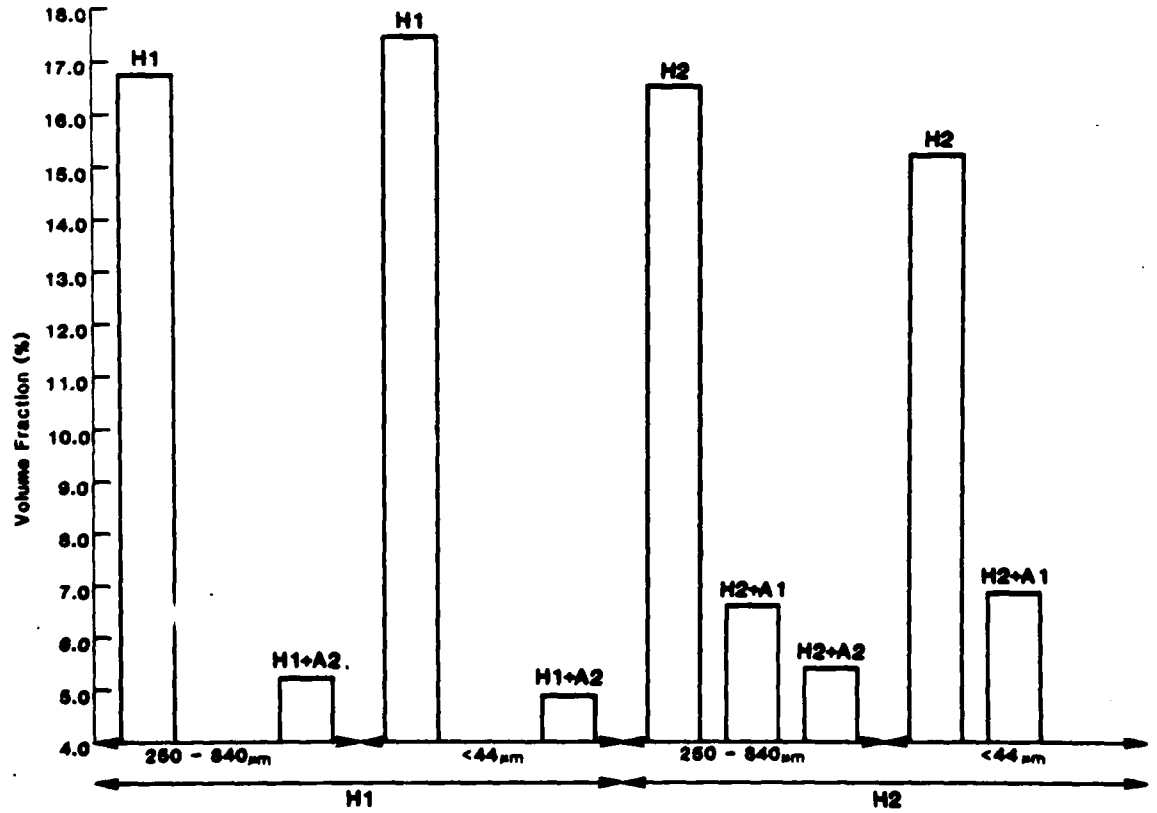

Figure 30. M_6C Carbide volume fraction (T15) as a function of powder screen fraction, HIPing temperature and austenitizing temperature.

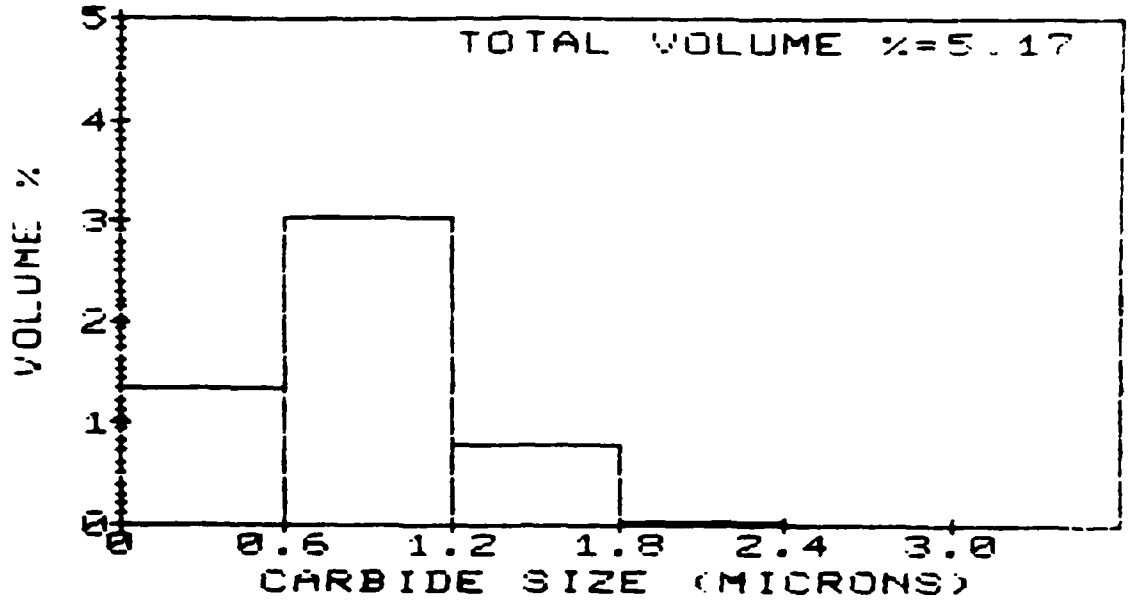

Figure 31. Size distribution - M_6C; H1 + A2/250-840 µm screen (T15).

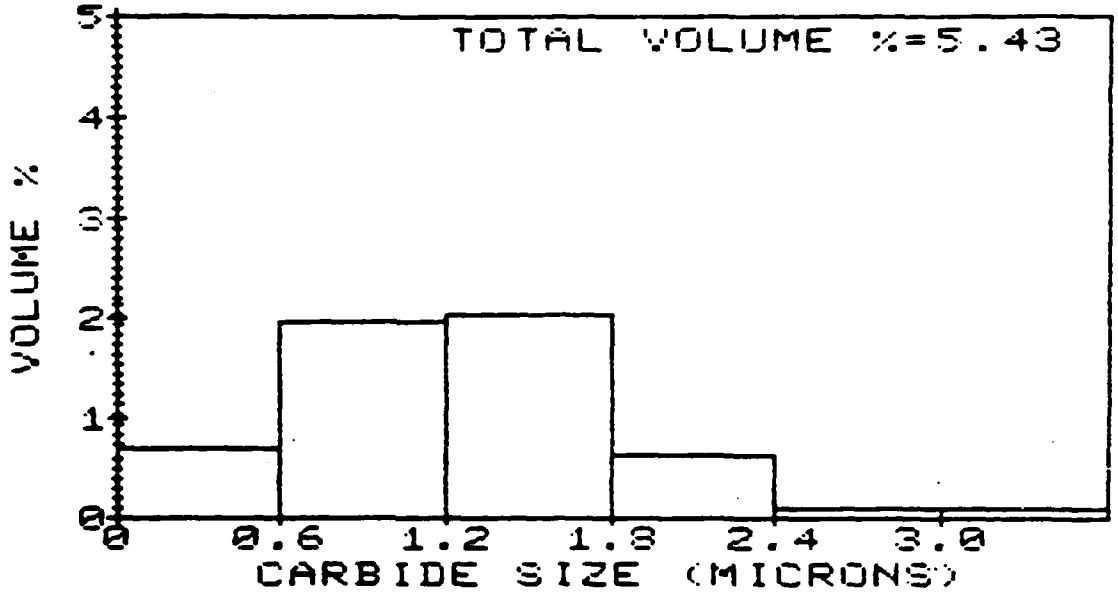

Figure 32. Size distribution - M_6C; H2 + A2/250-840 µm screen (T15).

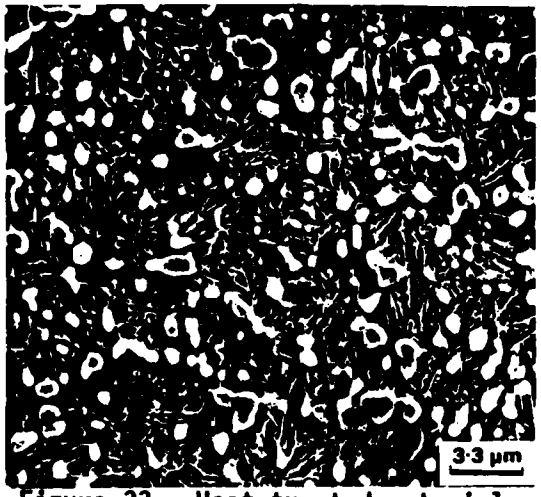

Figure 33. Heat-treated material; H2 + A1/250-840 µm screen (T15). Kalling's etch. SEM.

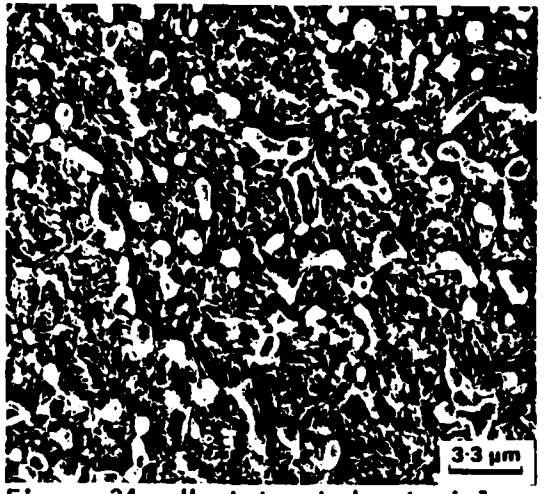

Figure 34. Heat-treated material; H2 + A1 + T1/250-840 µm screen (T15). Kalling's etch. SEM.

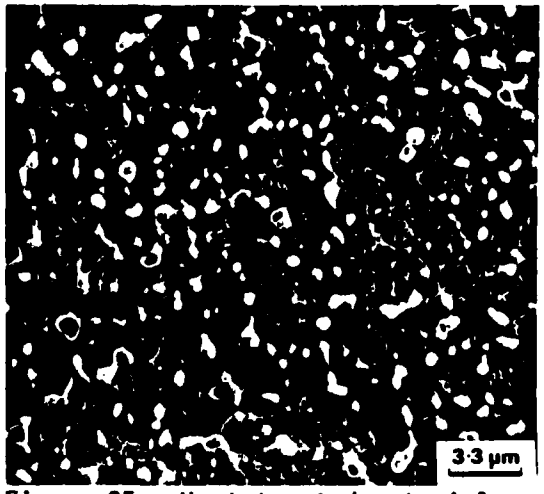

Figure 35. Heat-treated material; H2 + A1 + T3/250-840 µm screen (T15). Kalling's etch. SEM.

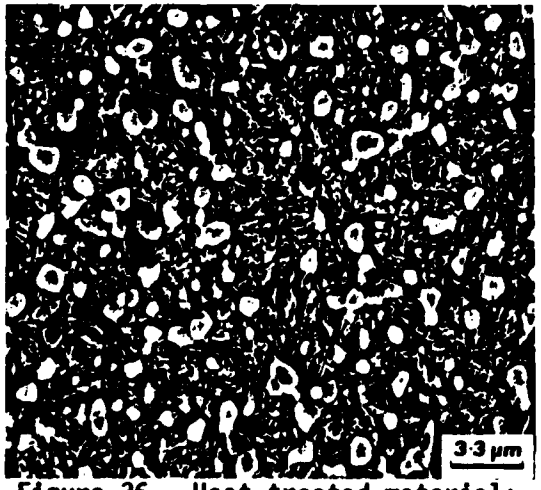

Figure 36. Heat-treated material; H2 + A1/≤ 44 µm screen (T15). Kalling's etch. SEM.

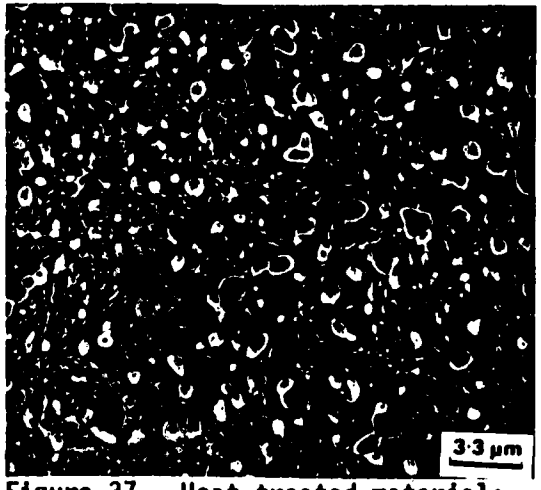

Figure 37. Heat-treated material; H2 + A1 + T1/≤ 44 µm screen (T15). Kalling's etch. SEM.

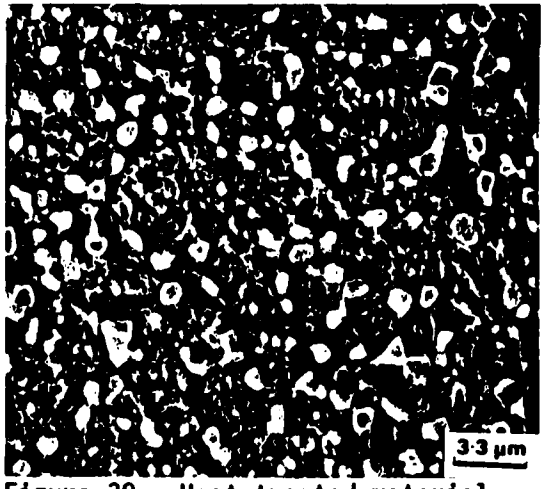

Figure 38. Heat-treated material; H2 + A1 + T3/≤ 44 µm screen (T15). Kalling's etch. SEM.

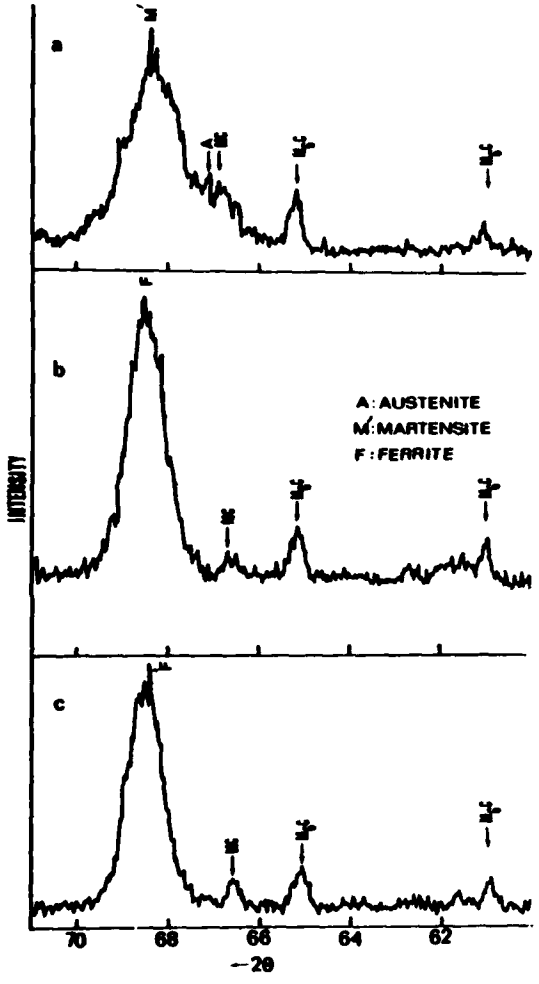

Figure 39. X-ray diffraction traces of heat-treated T15. (a) H2 + A1/250-840 μm screen. (b) H2 + A1 + T1/250-840 μm screen. (c) H2 + A1 + T3/250-840 μm screen.

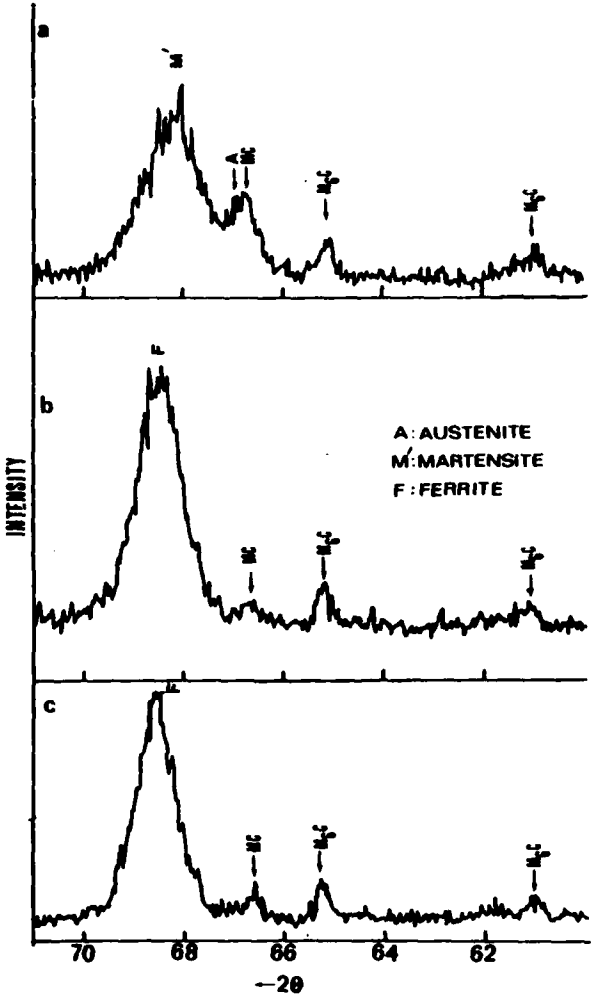

Figure 40. X-ray diffraction traces of heat-treated T15. (a) H2 + A2/250-840 μm screen. (b) H2 + A2 + T1/250-840 μm screen. (c) H2 + A2 + T3/250-840 μm screen.

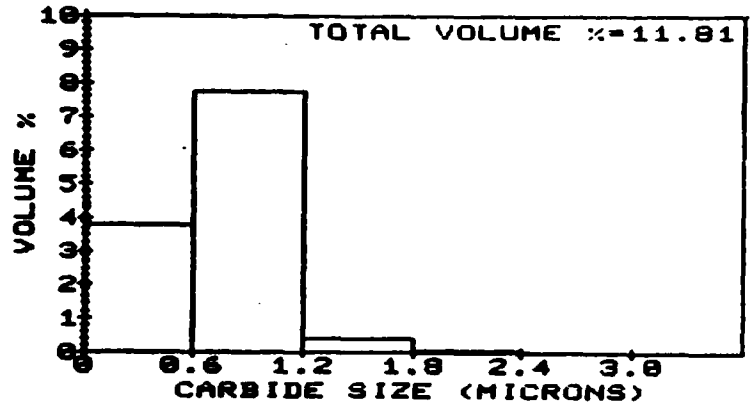

Figure 41. Size distribution - MC; H1 + A2 + T1/ 250-840 μm screen (T15).

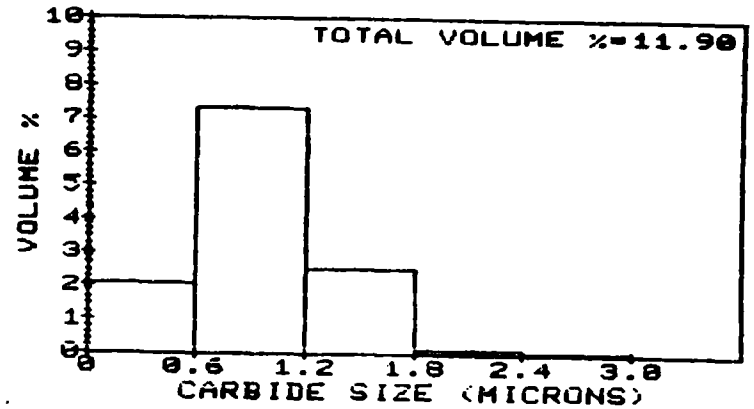

Figure 42. Size distribution - MC; H2 + A2 + T1/ 250-840 μm screen (T15).

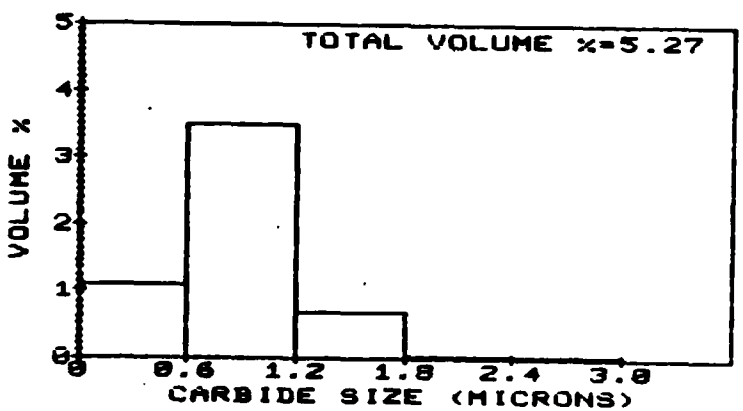

Figure 43. Size distribution - M_6C; H1 + A2 + T1/ 250-840 μm screen (T15).

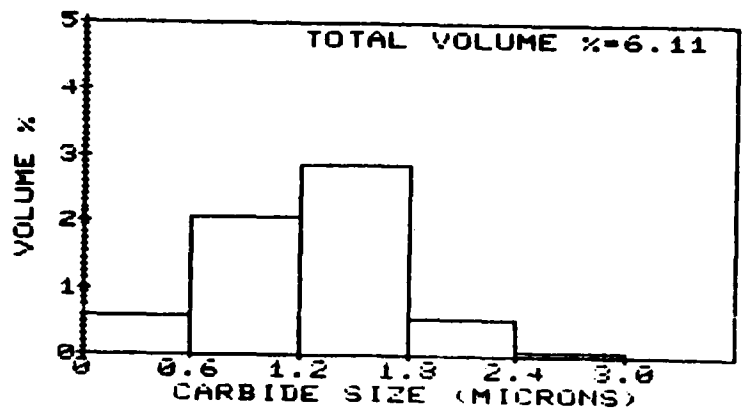

Figure 44. Size distribution - M_6C; H2 + A2 + T1/ 250-840 μm screen (T15).

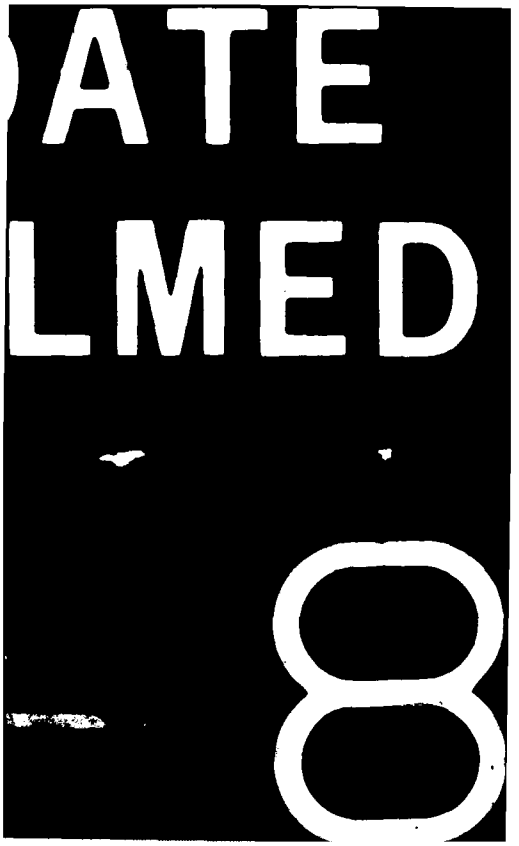
ATE
LMED
8